Japanese Journal of Applied Physics

BRIEF NOTE

Analysis of propagation characteristics of Rayleigh surface acoustic waves on $Yb_{0.33}Al_{0.67}N$ piezoelectric films/high-velocity substrates

To cite this article: Masashi Suzuki and Shoji Kakio 2022 *Jpn. J. Appl. Phys.* **61** SG1014

Japanese Journal of Applied Physics **61**, SG1014 (2022) **BRIEF NOTE**
https://doi.org/10.35848/1347-4065/ac48d2

Analysis of propagation characteristics of Rayleigh surface acoustic waves on $Yb_{0.33}Al_{0.67}N$ piezoelectric films/high-velocity substrates

Masashi Suzuki* and Shoji Kakio

Graduate Faculty of Interdisciplinary Research, University of Yamanashi, Kofu, Yamanashi 400-8511, Japan

*E-mail: masashis@yamanashi.ac.jp

Received November 2, 2021; revised December 18, 2021; accepted January 5, 2022; published online March 22, 2022

Piezoelectricity of YbAlN films has recently been shown to be almost as high as that of ScAlN films. YbAlN film surface acoustic wave (SAW) resonators are expected to have a high coupling factor. We theoretically investigated the propagation characteristics of first-mode Rayleigh SAWs (RSAWs) on $Yb_{0.33}Al_{0.67}N$ film/high-velocity Si, sapphire, AlN, SiC, BN, and diamond substrates. The first-mode RSAWs on the YbAlN layered structures had high coupling factors, higher than those on ScAlN layered structures. An enhancement of the effective coupling factor of the first-mode RSAWs was observed in polarity inverted YbAlN film/BN or diamond substrate structures.

Surface acoustic wave (SAW) resonators for frequency filters in future mobile communications and high-sensitivity sensors require a high coupling factor, high Q factor, high-frequency operation, and good temperature stability. It has recently been experimentally and theoretically demonstrated that leaky SAW, longitudinal leaky SAW, and high order mode Rayleigh-SAW (RSAW) resonators consisting of interdigital transducers (IDTs)/thin piezoelectric layers/high-velocity substrates[1–4] make it possible to achieve higher coupling factors than those for standard SAW resonators with IDTs/piezoelectric substrates. $LiNbO_3$ and $LiTaO_3$ thin plates, which have high piezoelectricity, are often used as the piezoelectric layers in these layered structure SAW resonators. A pure AlN piezoelectric film, which has a low mechanical loss, good temperature stability, high thermal conductivity, and high chemical stability, and thus enables operation in harsh environments, is also a good candidate for these piezoelectric layers. However, the coupling factors for AlN film SAW resonators are low because of the relatively small piezoelectric constants of the film.[5]

It has been reported that the piezoelectricity of AlN films is enhanced by Sc,[6–8] Yb,[9,10] Cr,[11,12] and MgZr[13] doping. In particular, the thickness extensional mode electromechanical coupling coefficient k_t^2 for AlN films is significantly improved by heavy Sc doing.[7] Layered structure SAW resonators with ScAlN films have a higher coupling factor than that for SAW resonators with AlN films.[14–17] The coupling factor for first-mode (Sezawa mode) RSAWs on the IDTs/c-axis oriented $Sc_{0.4}Al_{0.6}N$ film/diamond substrate is approximately four times higher than that for first-mode RSAWs on the IDTs/c-axis oriented pure AlN film/diamond substrate.[14] Yanagitani et al. experimentally demonstrated that the k_t^2 values for c-axis oriented YbAlN films were similar to those for c-axis oriented ScAlN films.[9] In addition, the elastic and piezoelectric constant tensors calculated using density functional theory for $Yb_{0.33}Al_{0.67}N$[10] are almost the same as those for $Sc_{0.4}Al_{0.6}N$.[18] We thus expect that RSAW resonators with YbAlN piezoelectric layers/high-velocity substrates will have high coupling factors, as is the case for ScAlN films. We demonstrated that the K^2 for the first-mode RSAWs on YbAlN film/high-velocity substrate were significantly higher than those of zeroth- and second-mode RSAWs on the YbAlN layered structures.[19]

In this study, the propagation characteristics of first-mode RSAWs on YbAlN film/high-velocity Si, sapphire, wurtzite AlN (wAlN), 6H-SiC, wurtzite BN (wBN), and diamond substrates were theoretically investigated in more detail. By comparing their characteristics with those of the ScAlN films, we discuss the advantage of YbAlN film RSAW resonators. The frequency characteristics for the first-mode RSAWs on IDTs/polarity inverted YbAlN films/substrates were simulated using a finite element method (FEM) analysis to estimate the effective coupling factor K_{eff}^2 for the RSAW resonators. In addition, the origins of the enhancement of the K_{eff}^2 for the polarity inverted structure were explored by observing the first-mode RSAW particle displacements in the polarity inverted YbAlN film RSAW resonators.

The phase velocities for first-mode RSAWs on (0°, 0°, 0°) $Yb_{0.33}Al_{0.67}N$ films/(0°, 0°, 0°) substrates were analyzed using Farnell and Adler SAW propagation analysis method.[20] The coupling factor K^2 was determined as

$$K^2 = 2^*(v_f - v_m)/v_f, \tag{1}$$

where v_f and v_m are the phase velocities on an electrically free surface and a metallized surface, respectively. The Yb content of the YbAlN film in this analysis was set to 33% because the piezoelectric constants (e_{33}, e_{31}, and e_{15}) were highest for $Yb_{0<x<0.4}Al_{1-x}N$.[10] The elastic constants, piezoelectric constants, and density for $Yb_{0.33}Al_{0.67}N$ calculated using density function theory[10] were used. Si ($v_f = 4900$ m s^{-1}),[21] sapphire ($v_f = 5550$ m s^{-1}),[22] wAlN ($v_f = 5700$ m s^{-1}),[23] 6H-SiC ($v_f = 6800$ m s^{-1}),[24] wBN ($v_f = 9600$ m s^{-1}),[25] and diamond ($v_f = 11\,000$ m s^{-1})[26] were selected as substrates because they have a higher RSAW phase velocity than that for $Yb_{0.33}Al_{0.67}N$ ($v_f = 3300$ m s^{-1}). As shown in Fig. 1(a), the phase velocities for the first-mode RSAWs on the YbAlN films/substrates decreased with increasing normalized YbAlN film thickness h/λ. As shown in Fig. 1(b), the K^2 values for first-mode RSAWs had a maximum of 6.3%–7.3% around h/λ =0.2–0.6. We analyzed the first-mode RSAWs characteristics on the $Sc_{0.4}Al_{0.6}N$ film/diamond substrate (dash line in Fig. 1) by using the same SAW analysis method as those for the YbAlN film/substrate structures. The K^2 values for first-mode RSAWs on the $Yb_{0.33}Al_{0.67}N$ film/substrate structure were higher than those for first-mode RSAWs on the $Sc_{0.4}Al_{0.6}N$ film/diamond structure. There were no significant differences in the elastic constants and the piezoelectric constants of $Yb_{0.33}Al_{0.67}N$[10] and $Sc_{0.4}Al_{0.6}N$[18] ($Yb_{0.33}Al_{0.67}N$: $c_{11} = 255$ GPa, $c_{12} = 139$ GPa, $c_{13} = 119$ GPa, $c_{33} = 192$ GPa, $c_{44} = 85$ GPa, $e_{33} = -0.21$, $e_{31} = -0.68$ and $e_{15} = 2.17$, $Sc_{0.4}Al_{0.6}N$: $c_{11} = 282$ GPa, $c_{12} = 137$ GPa, $c_{13} = 125$ GPa,

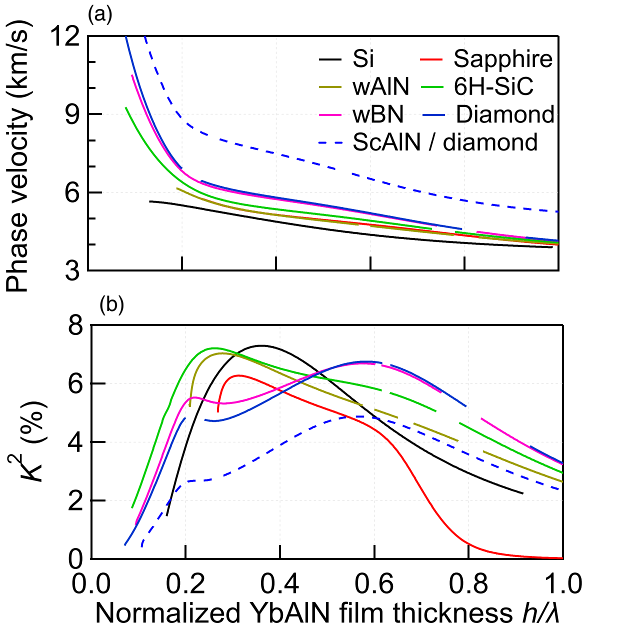

Fig. 1. (Color online) (a) Phase velocities and (b) K^2 values for first-mode SAWs on (0°, 0°, 0°) $Yb_{0.33}Al_{0.67}N$ films/Si, sapphire, wAlN, 6H-SiC, wBN, and diamond substrates as a function of normalized YbAlN film thickness h/λ.[19] The blue dashed lines indicate the phase velocity and K^2 on $Sc_{0.4}Al_{0.6}N$ film/diamond substrate.

$c_{33} = 169$ GPa, $c_{44} = 98$ GPa, $e_{33} = -0.29$, $e_{31} = -0.52$ and $e_{15} = 2.72$). However, the density of 5935 kg m^{-3} for $Yb_{0.33}Al_{0.67}N$[10] is approximately 1.7 times higher than that of 3601 kg m^{-3} for $Sc_{0.4}Al_{0.6}N$,[27] which causes the lower RSAW phase velocity of approximately 3300 m s^{-1} on $Yb_{0.33}Al_{0.67}N$ than that of approximately 4700 m s^{-1} on $Sc_{0.4}Al_{0.6}N$. We surmise that the large phase velocity difference between the piezoelectric $Yb_{0.33}Al_{0.67}N$ layer and the substrate induced a strong SAW particle concentration at the piezoelectric layer, which led to the high K^2 values, in the YbAlN film/high-velocity substrate structures.

Polarity inverted structures enhance the coupling factors for first-mode RSAWs on ScAlN or AlN films/diamond substrates.[28] This enhancement is also expected for YbAlN film/high-velocity substrate structures. We simulated the admittance frequency characteristics of the first-mode RSAWs on Al IDTs/(0°, 0°, 0°) YbAlN layers/(0°, 180°, 0°) YbAlN layers/substrates using FEM analysis (Femtet, Murata Software). Figure 2(a) shows the FEM analysis model for the layered structure SAW resonators. A perfect matching layer was assumed for the substrate bottom to remove the effect of reflected bulk waves from the substrate bottom. A periodic boundary was applied to both sides of the models. When the period of the infinite periodic Al IDTs was $\lambda = 8\ \mu$m, the substrate thickness and the film thickness for the Al IDTs were adjusted to be approximately 10λ and 0.01λ, respectively. The mechanical loss and dielectric loss (tanδ) for the YbAlN films and substrates were not taken into consideration. The total normalized YbAlN film thicknesses ($h_{1st}/\lambda + h_{2nd}/\lambda$) for the first-layer and second-layer thicknesses were fixed at 0.36, 0.31, 0.28, 0.26, 0.58 and 0.58 on Si, sapphire, wAlN, 6H-SiC, wBN, and diamond substrates, respectively. These $h_{1st}/\lambda + h_{2nd}/\lambda$ values led to the highest K^2 value for the first-mode RSAWs on the monolayer YbAlN film/substrate, as shown in Fig. 1(b). The h_{1st}/λ and h_{2nd}/λ

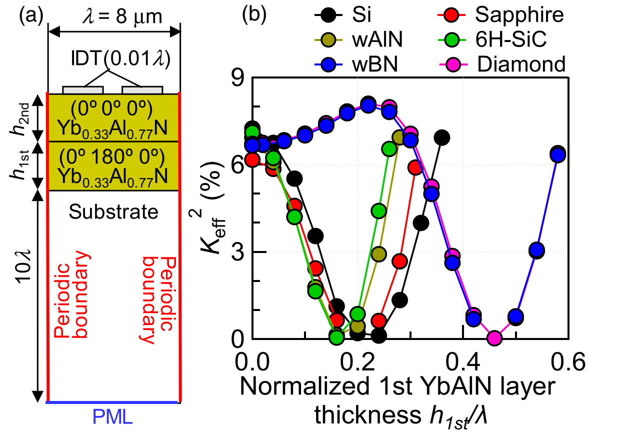

Fig. 2. (Color online) (a) FEM model of Al IDTs/polarity inverted YbAlN film/substrate. (b) K_{eff}^2 values for first-mode RSAWs on polarity inverted YbAlN films/Si, sapphire, wAlN, 6H-SiC, wBN, and diamond substrates as a function of normalized first-layer thickness h_{1st}/λ.[19]

values varied in the range of 0.00 to $h_{1st}/\lambda + h_{2nd}/\lambda$. The K_{eff}^2 values for first-mode RSAWs were obtained from the resonance and anti-resonance frequencies of the admittance frequency characteristics. As shown in Fig. 2(b), the K_{eff}^2 values for the polarity inverted YbAlN films/Si, sapphire, wAlN, and 6H-SiC substrates decreased with increasing h_{1st}/λ (from 0 to 0.16–0.24). Above $h_{1st}/\lambda = 0.16$–0.24, the K_{eff}^2 values gradually increased to the K_{eff}^2 values at $h_{1st}/\lambda = 0.00$. The K_{eff}^2 values for the polarity inverted YbAlN films/wBN and diamond substrates increased with increasing h_{1st}/λ (from 0 to 0.22). The maximum K_{eff}^2 values (approximately 8.0%) at $h_{1st}/\lambda = 0.22$ were approximately 1.2 times higher than those for the monolayer YbAlN films/wBN and diamond substrates at $h_{1st}/\lambda = 0.00$. Next, we observed the SAW particle displacements for first-mode RSAWs on the polarity inverted YbAlN film or monolayer YbAlN film/diamond or Si substrate. As shown in Figs. 3(a) and 3(b), for the polarity inverted YbAlN film ($h_{1st}/\lambda = 0.22$)/diamond substrate with high K_{eff}^2 of 8.0%, the SAW particles of the first-mode RSAWs were strongly concentrated at the YbAlN piezoelectric layer. In addition, the SAW evanescence to the substrate observed around the interface between the YbAlN film and the substrate was more suppressed. We confirmed that the depth from the YbAlN film surface, where the first-mode RSAW particles were concentrated, did not change in the monolayer and polarity inverted YbAlN films/diamond substrates. The highest K_{eff}^2 value was obtained by setting the boundary between the polarity inverted structure at the depth where the first-mode RSAW particles were concentrated. As shown in Figs. 3(c) and 3(d), for the YbAlN film/Si substrate structures, most of the first-mode RSAW particles were in the Si substrate. Therefore, the polarity inverted structure in the YbAlN film may adversely affect first-mode RSAW propagation and the K_{eff}^2 values for the polarity inverted YbAlN film/Si substrate. Furthermore, in the polarity inverted YbAlN film ($h_{1st}/\lambda = 0.24$)/Si substrate with small K_{eff}^2 of 0.1%, the strong SAW particle concentration did not appear in the YbAlN films and the interface between IDTs and YbAlN film, and the SAW leakage to the Si substrate were slightly enhanced. From these observations, we conclude that the piezoelectricity of the YbAlN film contributes little to the

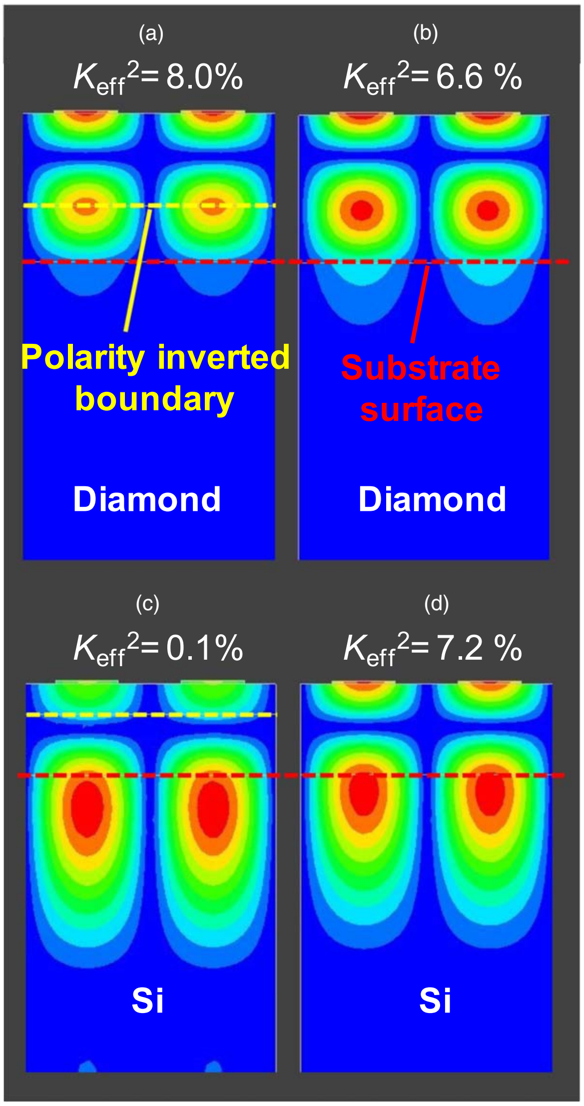

Fig. 3. (Color online) Particle displacements for first-mode RSAWs in z direction at resonance frequency on (a) polarity inverted YbAlN film/diamond substrate, (b) monolayer YbAlN film/diamond substrate, (c) polarity inverted YbAlN film/Si substrate, and (d) monolayer YbAlN film/Si substrate.

SAW propagation on the polarity inverted YbAlN film/Si substrate, which leads to the small K_{eff}^2 value.

In conclusion, the propagation characteristics of the first-mode RSAWs on YbAlN films/high-velocity Si, sapphire, w-AlN, 6H-SiC, w-BN, and diamond substrates were analyzed. We demonstrated that all YbAlN layered structures had high K^2 values for first-mode RSAWs which were higher than that of ScAlN film/diamond substrate. Moreover, the K_{eff}^2 value for the first-mode RSAWs was enhanced in the polarity inverted YbAlN film/BN or diamond substrate.

Acknowledgments This work was supported by a Japan Society for the Promotion of Science Grant-in-Aid for Early-Career Scientists (Grant No. 19K15024), Scientific Research B (Grant No. 19H02202 and 20H02181), and the IZUMI Science and Technology Foundation.

ORCID iDs Masashi Suzuki https://orcid.org/0000-0002-7044-9474 Shoji Kakio https://orcid.org/0000-0002-5776-1383

1) M. Gomi, T. Kataoka, J. Hayashi, and S. Kakio, Jpn. J. Appl. Phys. **56**, 07JD13 (2017).
2) M. Kadota and S. Tanaka, Jpn. J. Appl. Phys. **57**, 07LD12 (2018).
3) N. Naumenko, Ultrasonics **95**, 1 (2019).
4) S. Inoue and M. Solal, Proc. IEEE Ultrason. Symp., p. 2079 (2019).
5) S. Sikata, H. Nakahata, and A. Hachigo, New Diamond Front. Carbon Technol. **9**, 75 (1999).
6) M. Akiyama, T. Kamohara, K. Kano, A. Teshigahara, Y. Takeuchi, and N. Kawahara, Adv. Mater. **21**, 593 (2008).
7) M. Suzuki, T. Yanagitani, and H. Odagawa, Appl. Phys. Lett. **104**, 172905 (2014).
8) T. Yanagitani and M. Suzuki, Appl. Phys. Lett. **105**, 122907 (2014).
9) T. Yanagitani and M. Suzuki, US Patent Application US10763816B2 (2019).
10) J. Jia and T. Yanagitani, Phys. Rev. Appl. **16**, 044009 (2021).
11) S. Manna, K. R. Talley, P. Gorai, J. Mangum, A. Zakutayev, G. L. Brennecka, V. Stevanović, and C. V. Ciobanu, Phys. Rev. Appl. **9**, 034026 (2018).
12) Y. Takano, R. Hayakawa, M. Suzuki, and S. Kakio, Jpn. J. Appl. Phys. **60**, SDDC08 (2021).
13) T. Yokoyama, Y. Iwazaki, Y. Onda, T. Nishihara, Y. Sasajima, and M. Ueda, IEEE Trans. Ultrason. Ferroelectr. Freq. Contr. **61**, 1322 (2014).
14) K. Hashimoto, T. Fujii, S. Sato, T. Omori, C. Ahn, A. Teshigawara, K. Kano, H. Umezawa, and S. Shikata, Proc. IEEE Ultrason. Symp., p. 1, 2012.
15) M. Suzuki, M. Gomi, and S. Kakio, Jpn. J. Appl. Phys. **57**, 07LD06 (2018).
16) M. Suzuki, N. Sawada, and S. Kakio, Jpn. J. Appl. Phys. **58**, SGGC08 (2019).
17) M. Suzuki and S. Kakio, Jpn. J. Appl. Phys. **59**, SKKC07 (2020).
18) M. A. Caro, S. Zhang, M. Yliammi, T. Reikkinen, M. A. Moram, O. L. Acevedo, J. Molarius, and T. Laurila, J. Phys. Condens. Matter **27**, 279602 (2015).
19) M. Suzuki and S. Kakio, Proc. Symp. Ultrasonic Electronics 2021, p. 2E1-3.
20) G. W. Farnell and E. L. Adler, in *Physical Acoustics*, ed. W. P. Mason and R. N. Thurston, (Academic, New York, 1972) , p. 35.
21) M. Shibayama, *Danseiha Device Gijutsu Handbook* (Ohmsha, Tokyo, 1991) Acoustic Wave Device Technology Handbook, p. 546, [in Japanese].
22) M. Shibayama, *Danseiha Device Gijutsu Handbook* (Ohmsha, Tokyo, 1991) Acoustic Wave Device Technology Handbook, p. 544, [in Japanese].
23) Y. Ohashi, M. Arakawa, J. Kushibiki, B. M. Epelbaum, and A. Winnacker, Appl. Phys. Exp. **1**, 077004 (2008).
24) K. Kamitani, M. Grimsditch, J. C. Nipko, C.-K. Loong, M. Okada, and I. Kimura, J. Appl. Phys. **82**, 3152 (1997).
25) K. Shimada, Jpn. J. Appl. Phys. **45**, L358 (2006).
26) K. Yamanouchi, N. Sakurai, and T. Satoh, Proc. IEEE Ultrason. Symp., p. 351, 1989.
27) A. Konno, M. Kadota, J. Kushibiki, Y. Ohashi, M. Esashi, Y. Yamamoto, and S. Tanaka, Proc. IEEE Ultrason. Symp., p. 273, 2014.
28) T. Yanagitani and S. Takayanagi, Jpn. J. Appl. Phys. **60**, SD0803 (2021).